https://doi.org/10.1002/bit.26221

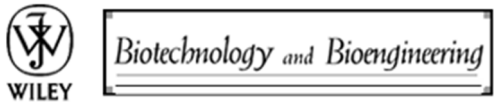

Shuttle-mediated nanoparticle transport across an in vitro brain endothelium under flow conditions

Journal:	*Biotechnology and Bioengineering*
Manuscript ID	16-739.R1
Wiley - Manuscript type:	Article
Date Submitted by the Author:	n/a
Complete List of Authors:	Falanga, Andrea; Istituto Italiano di Tecnologia Center for Advanced Biomaterials for Healthcare, Center for Advanced Biomaterials for Healthcare; Universita degli Studi di Napoli Federico II, Department of Chemical, Materials and Industrial Production Engineering, and Interdisciplinary Research Centre for Biomedical Materials Pitingolo, Gabriele; Istitutto Italiano di Tecnologia, Center for Advanced Biomaterials for Healthcare Celentano, Maurizio; Istituto Italiano di Tecnologia Center for Advanced Biomaterials for Healthcare, Center for Advanced Biomaterials for Healthcare Cosentino, Armando; Istituto Italiano di Tecnologia Center for Advanced Biomaterials for Healthcare, Center for Advanced Biomaterials for Healthcare Melone, Pietro; Istituto Italiano di Tecnologia Center for Advanced Biomaterials for Healthcare, Center for Advanced Biomaterials for Healthcare Vecchione, Raffaele; Istituto Italiano di Tecnologia, Center for Advanced Biomaterials for health Care (CABHC) Guarnieri, Daniela; Center for Advanced Biomaterials for health Care (CABHC), Istituto Italiano di Tecnologia Netti, Paolo; University of Naples, Interdisciplinary Research Centre on Biomaterials
Key Words:	blood brain barrier, microfluidics, nanoparticles, membranotropic peptides, flow conditions

Biotechnology & Bioengineering
https://doi.org/10.1002/bit.26221

Shuttle-mediated nanoparticle transport across an *in vitro* brain endothelium under flow conditions

RUNNING TITLE: Functionalized-NP transport through a BBB on a chip

Andrea P. Falanga[1], Gabriele Pitingolo[1], Maurizio Celentano[1], Armando Cosentino[1], Pietro Melone[1], Raffaele Vecchione[1,*], Daniela Guarnieri[1,*], Paolo A. Netti[1,2,3]

[1]*Center for Advanced Biomaterial for Health Care (CABHC), Istituto Italiano di Tecnologia, Largo Barsanti e Matteucci 53, Napoli, Italy*

[2]*Centro di Ricerca Interdipartimentale sui Biomateriali (CRIB), Università di Napoli Federico II, Piazzale Tecchio 80, Napoli, Italy*

[3]*Dipartimento di Ingegneria, Università di Napoli Federico II, Piazzale Tecchio 80, Napoli, Italy*

* Corresponding authors: daniela.guarnieri@iit.it ; raffaele.vecchione@iit.it

https://doi.org/10.1002/bit.26221

Abstract

The blood brain barrier (BBB) represents a challenge in the development of new nano-delivery systems able to reach the central nervous system (CNS). In order to test the efficacy of these nanocarriers, it is fundamental to use *in vitro* models that resemble the *in vivo* cell culture conditions. Here, we demonstrate for the first time the ability of a membranotropic peptide, namely gH625, to transport a cargo -acting as a shuttle- across the BBB layer under flow conditions that mimic the blood flow rate. To this aim, a BBB microfluidic device was designed based on a transparent polyester porous membrane sandwiched between a top and a bottom overlying channel made of poly(methyl methacrylate) (PMMA). Our data clearly indicate that this microfluidic system allows the growth of brain endothelial bEnd.3 cells and the formation of a confluent layer at 7 days of culture that hinders the passage of nanoparticles compared to porous membrane alone. The device was validated at a 5 µl/min working flow rate, where the capability of the model to remain intact after nanoparticle passage was shown. Very interestingly, the decoration with the gH625 peptide enhances the adhesion of nanoparticles to the endothelial layer and the BBB crossing in flow conditions, thus confirming the efficacy of the gH625 as a delivery platform to the brain.

Keywords: blood brain barrier, microfluidics, nanoparticles, membranotropic peptides, flow conditions

https://doi.org/10.1002/bit.26221

Introduction

The blood-brain barrier (BBB) with its distinctive tissue architecture acts as a formidable filter to separate the peripheral blood from the central nervous system (CNS), thereby maintaining brain homeostasis (Cardoso et al. 2010; Paolinelli et al. 2011). The permeability of the BBB is controlled, among others, by the brain endothelial cells that regulate the selective transport from the blood to the brain and *vice versa* (Cardoso et al. 2010). The endothelial layer is also crucial in preventing the entrance of toxic substances to the brain (Paolinelli et al. 2011). Due to this tight barrier, the majority of drugs fail to cross the BBB and to exert their therapeutic effects. For this reason, the main challenge for the improvement of new drug delivery systems is represented by their ability to overcome the BBB, and many efforts in this field are currently devoted to increase the uptake of therapeutic compounds into the brain parenchyma. We have recently demonstrated that the conjugation with the membranotropic peptide gH625 enables the transport of nanoparticles (NPs) across the BBB, leading to a significantly higher cell uptake and crossing, and, most importantly, to a reduction of NP intracellular accumulation as large lysosomal aggregates in a static BBB model (Guarnieri et al. 2013). The hydrophobic nature of gH625, which derives from the glycoprotein H (gH) of Herpes simplex virus 1, allows the efficient interaction with biological membranes helping lipid membrane-reorganizing processes, such as fusion or pore formation, thus inducing temporary membrane destabilization and subsequent reorganization (Galdiero et al. 2007). This class of hydrophobic molecules has recently gained a lot of attention since they may be used for drug delivery purposes. In particular, the nineteen residues of the gH625 peptide provide membrane-perturbing properties (Galdiero et al. 2005; Galdiero et al. 2010; Raiola, et al. 2008; Vitiello et al. 2011) enabling the interaction with model membranes, promoting their merging (Falanga et al. 2011) and have shown the capability to penetrate the membrane bilayer and transport cargoes into the cytoplasm and across the brain endothelium of an *in vitro* BBB Transwell system (Guarnieri et al. 2013).

Most of the experiments aiming at studying the transport of materials through the BBB are usually performed using static Transwell assays (Avdeef et al. 2011; Hatherell et al. 2011; Patabendige et al. 2013). However, *in vivo* brain endothelial cells are subjected to the blood flow that is absent in these commonly used *in vitro* models. *In vivo* models would be ideal to study the transport across the BBB, but they are limited, expensive and hard to study both in detail and real-time. Additionally, animal experiments inevitably include several unquantified variables, such as animal health status, reproducible growth, diet, weight, and intrinsic genetic differences. *Ex vivo* and new *in vitro* models represent valid alternatives for their simplicity and controlled environment (Cardoso et al. 2010; Cucullo et al. 2005).

Recently, the use of microtechnologies to study organ physiology has received a rapidly growing attention (Huh et al. 2011; Vecchione et al. 2016) as an *in vitro* tool. These organs-on-chips have the potential to be used as human-relevant disease models, and additionally provide detailed insights into drug effects (Huh et al. 2011; van der Meer et al. 2010). Some microfluidic models of the BBB have recently been reported, demonstrating the feasibility of an organ-on-chip approach (Booth & Kim 2012; Yeon et al. 2012; Wang et al. 2016).

The possibility to study/predict the behavior of functionalized nanoparticles in brain endothelium in experimental models that mimic blood flow conditions could, therefore, provide new insights in the design of efficient drug delivery platforms to the brain.

In this context, the aim of this work was to test the ability of the gH625 peptide to transport nanoparticles across the brain endothelium under flow conditions. To mimic the blood flow in brain capillaries, we designed an *in vitro* microfluidic BBB model. The system was created in such a way as to permit the growth of the cells on a porous filter up to reaching the confluence and to separate two compartments delimited by the endothelial layer, that is the blood side and the brain side. The microfluidic chip (Figure 1) contains a transparent polyester microporous membrane sandwiched between a top and a bottom overlying channel. The endothelial layer is obtained on the porous

https://doi.org/10.1002/bit.26221

membrane directly into the device after culturing mouse brain endothelial bEnd.3 cells. A collecting chamber is also integrated on the top channel in order to collect transported NPs and to allow oxygen exchange.

We first characterized the growth and the formation of a confluent brain endothelial layer within the *in vitro* microfluidic system through the measurement of the trans-endothelial electrical resistance (TEER) and through bright-field and confocal microscopy observations. Then, we evaluated the transport across the microfluidic BBB of amine-modified fluorescent polystyrene nanoparticles - chosen as control particles- and the capability of gH625-conjugated nanoparticles to adhere to and cross the brain endothelial layer under flow conditions compared to the control.

Materials and methods

Microfluidic system design and fabrication

In this section, we detail the design and fabrication of the microfluidic chip. It is based on different poly(methyl methacrylate) (PMMA) layers 1.2 mm thick and purchased from Goodfellow Cambridge Ltd, (UK) which were bonded via solvent evaporation. Specifically, the assembly of the PMMA layers was performed by simply immersing PMMA substrates in ethanol for 10 min. The immersed substrates were immediately removed, aligned and clamped for an overlap of the top and bottom channel, then the heat treatment was initiated at 58 °C for 45 minutes. Before proceeding with the assembly of the chip the manufacturing substrates were cleaned using a common soap (RBS Ditalclean, Brussels). The bonding between the top channel substrate and the bottom channel substrate allows enclosing the polyester membrane (Corning Costar, Cambridge, MA, USA; 3 µm porous size) on which cells are grown afterwards. PMMA is a transparent thermoplastic polymer that can be easily micromachined by micromilling (Minitech Machinery Corporation) which is a fast prototype technique (Chen et al. 2014). In addition to bond NanoPorts Upchurch® to PMMA

microdevices, we developed a hybrid system, which glues commercial nanoports with an alternative biocompatible epoxy adhesive. The microfluidic chip shown in Figure 1 is composed of two PMMA channel substrates (12 x 50 x 1 mm) and a PMMA collecting chamber (12 x 30 x 1 mm). The size of the channel is different onto the two PMMA channel substrates, 889 µm of width and depth and 36 mm of length for the bottom channel and 1 mm of depth, 889 µm of width and 6 mm of length for the top channel. The collecting chamber was 6 x 10 x 1 mm (width x length x depth). Moreover, we fabricated two microchannels connected to the top and bottom channel with holes to integrate the electrodes. Pt electrodes were fabricated by sputter deposition of 20 nm of platinum on the surface of metallic metal blunt needles named hypo needles 18 AWG purchased from Warner Instruments and characterized by a 1.3 mm of external diameter (Figure S1). The microtool used to micromachine the PMMA was in all the cases a flute endmill with an 889 µm diameter. In the second PMMA layer we microfabricated inlet and outlet holes to connect microfluidic chips with classic fluidic equipment such as syringe pump and tubing. The fabrication process consisted of 4 steps: (1) preparation of the chip draft using Draftsight (Cad Software), (2) micromachining of PMMA layers; (3) ethanol-assisted bonding process and (4) bonding Nanoport Upchurch to PMMA substrate. The certified positioning accuracy of the three-axis are 12”/300 mm in x-axis, 9”/228 mm in y-axis, and 9”/228 mm in z-axis. To standardize the fabrication process, the PMMA substrates used in this study were purchased from the same batch of the polymer supplier (GoodFellow Cambridge Limited, England).

Cell culture

Mouse cerebral endothelial bEnd.3 cells (American Type Culture Collection, Manassas, VA) were grown in DMEM with 4.5 g/l glucose, 10% Foetal Bovine Serum (FBS), 3.7 g/l sodium bicarbonate, and 4 mM glutamine, 1% non-essential amino acids, 100 U/ml penicillin and 0.1 mg/ml streptomycin in 100 mm diameter cell culture dish, in a humidified atmosphere at 37 °C and 5% CO_2. Cells used in all experiments were at passage 11–18.

https://doi.org/10.1002/bit.26221

Cell seeding and culture in the microfluidic system

The fabricated chip had been previously sterilized with 10% Penicillin-Streptomycin solution for 24 h at 4 °C to prevent contamination. bEnd.3 cells were seeded at a density of 25×10^3 cells/cm^2 into a microfluidic channel and the system was upside down, in order to allow cell adhesion to the polyester filter located on the top of the channel. Non-adhered cells were removed 24 h after seeding by twice washing with fresh cell culture medium. Afterward, cells were allowed to grow until 7 days within the device. Medium was refreshed every 3 days. Cell growth was monitored over time by phase contrast and confocal microscopy at 1, 3, 5 and 7 days of culture. To evaluate cell confluence and tight junction integrity, TEER levels were measured every day after cell seeding until day 7 of cell culture.

In order to further verify cell growth in the microfluidic system, bEnd.3 cells were fixed by pouring 4% paraformaldehyde directly into the system channel and incubating for 10 min at RT. Cells were then stained with 4',6-diamidino-2-phenylindole (DAPI, Sigma), hence, the number of nuclei was counted by ImageJ software 1.44p.

Trans-endothelial electrical resistance (TEER) measurements

TEER measurements were carried out by connecting the BBB chip to an AUTOLAB PGSTAT302N (potentiostat/galvanostat) equipped with a FRA32M module (frequency response analysis module). Impedance spectra were recorded in potentiostatic mode with an amplitude of 0.01 V and frequencies ranging from 100 kHz to 0.1 Hz between two Pt electrodes. For each measurement 3 readings and 50 data points (logarithmic frequency step) per reading were collected. The least-square optimization method was used to fit the measured impedance data to an electrical equivalent circuit model, reported in Figure 4 A. In the adopted model the constant phase element represents the dual layer capacitance of Pt electrodes (C_{El}), which is in series with the resistance of the medium (R_{medium}) and the cell layer, which is denoted as the resistance of cells (R_{TEER}) and the

https://doi.org/10.1002/bit.26221

capacitance of the cell membranes (C_{Cl}) in parallel. The porous polymeric membrane used as supporting material for cells adhesion and growing represents an additional resistive term (R_{mem}), which is in parallel with R_{TEER}. Thus, for each impedance spectra an apparent R_{TEER} (R_{eq}) was collected and then corrected (eq. 1) for the membrane resistance to obtain the effective R_{TEER}.

$$R_{TEER} = \frac{R_{eq} \times R_{mem}}{R_{eq} - R_{mem}} \qquad \text{eq. 1}$$

R_{TEER} was normalized for the cross sectional surface area of the chip (0.054 cm^2) to calculate TEER value in Ohm*cm^2.

Cell staining

The presence of tight junctions was determined by immune-staining with anti-Claudin 5 antibody (Life Technologies). Briefly, bEnd.3 cells were fixed with 4% paraformaldehyde for 10 minutes. After permeabilization with 0.1 % Triton-X100, cells were incubated with the blocking buffer (BB) (0.5% BSA in PBS) and were stained with the anti-Claudin 5 primary antibody for 1 h at RT. Then, the Alexa-488 anti-Mouse secondary antibody diluted in BB was incubated 1 h at RT.

In order to detect actin filaments, TRITC-Phalloidin (Sigma) was used. After fixation and permeabilization, bEnd.3 cells were incubated for 30 minutes at RT. DAPI was used for nuclei staining. All samples were then observed at confocal microscope (Leica TCS SP5 MP) with a 25 × water-immersion objective.

Blank and gH625-functionalized nanoparticles

Orange fluorescent amine-modified polystyrene nanoparticles with a 100 nm diameter (Sigma-Aldrich) were used as blank nanoparticles. The same nanoparticles were covalently conjugated to the gH625 peptide (Ac-HGLASTLTRWAHYNALIRAFGGG-COOH). The peptide was synthesized using the standard solid-phase-9-fluorenylmethoxycarbonyl (Fmoc) method (Rusciano et al. 2011) as previously reported (Galdiero et al. 2005). The gH625 peptide conjugation to the

https://doi.org/10.1002/bit.26221

nanoparticles was performed according to EDC/NHS procedure as described previously (Guarnieri et al. 2013). Mean size, size distribution and zeta-potential of blank and gH625-nanoparticles were characterized by a Zetasizer Nano-ZS (Malvern Instruments, Worcestershire, UK). NP morphology before and after functionalization was observed by transmission electron microscopy (TEM) (TECNAI G2, FEI). Results of NP characterization are reported in Table S1 and Figure S2.

Transport assay

Transport experiments across the BBB microfluidic system were performed at day 7 after seeding. Briefly, a 5 ml syringe was loaded with a FITC-BSA solution at the final concentration of 0.1 mg/ml in cell culture medium supplemented with 40 mM HEPES buffer. For nanoparticle transport experiments, the syringe was loaded with blank and gH625-NP suspensions in buffered cell culture medium at the final concentration of 9.20×10^{10} and 1.84×10^{10} NP/ml. The syringe was then allocated on a syringe pump (Harvard Apparatus Pump 11 Elite) connected to the inlet of the microfluidic system by a tube (Radel Tubing 1/16x020xsoft). The outlet of the system was connected to an Eppendorf tube through the same kind of tube in order to collect the output flow media. The collection chamber was filled with 90 µl of cell culture medium. The experiments were carried out in a plexiglass incubator at 37 °C and solutions flowed at 5 or 25 µl/min flow rates. Compounds and NPs that cross the endothelial layer were collected in the apical chamber. Experiments were carried out for 3 hours, drawing the medium in the collection chamber every 30 minutes and replacing it with fresh medium. The transport of BSA and nanoparticles across the BBB layer was estimated by fluorescence measurements through a spectrofluorometer (Perkin-Elmer, USA). Data were reported as the percentage of transported BSA and NPs compared to the initial concentrations of the fluorescent compounds.

Image analysis

https://doi.org/10.1002/bit.26221

In order to quantify the amount of NPs in the cells, after NP transport experiment under flow conditions, bEnd.3 cells were fixed in the microfluidic system and stained with DAPI. Five images for each sample were acquired by confocal microscope and analyzed. The quantification of fluorescent NPs was performed by using area calculator plugins of ImageJ software. Data were reported as fluorescent areas normalized to the number of the cell nuclei.

Statistical analysis

Results were expressed as mean ± standard deviation (SD). Results repeats were compared by a one-way analysis of variance (ANOVA), and a p value < 0.05 was considered statistically significant.

Results and discussion

In vitro BBB model characterization

The microfluidic device was tested before cell seeding in terms of sealing by fluxing fluids at different flow rates ranging from 1 µl to > 1 ml/min and no leakage was observed. It was also morphologically characterized by SEM in order to confirm the right alignment and dimensions of the channels (Figure 1 C).

Simulations based on the Finite Element Method (FEM) were performed to verify the spontaneous direction of the vertical flow through a permeable layer in place of the brain endothelial layer. To this aim, a simplified model based on the Navier Stokes equations in porous media was introduced (see Supporting info for details). In our system, on the one hand the gravity force, acting in the upper reservoir, tends to move the liquid downward; on the other hand, the pressure in the bottom channel tends to move the liquid in the opposite direction. From the simulations it resulted that in permeability conditions the liquid/air interface in the reservoir tends to move downward (Figure

https://doi.org/10.1002/bit.26221

S3). In this scenario, we were able to exclude any particle transmigration from the bottom microchannel to the upper chamber due to fluid extravasation since the flow went spontaneously to the opposite direction.

bEnd.3 cells were seeded in the channel and allowed to adhere to the membrane for 24 h at 37 °C. Afterward, the system was upside down, the channel was rinsed with fresh medium to remove non-adhered cells and incubated at 37 °C for 1, 3 and 7 days of culture. Figure 2 shows phase contrast images of the bEnd.3 cell layer after different days of growth in the microfluidic device. As reported, cell confluence increased over time. Seven days post cell seeding the cells formed a confluent layer as demonstrated by the nuclei and microfilament fluorescent staining (Figure 3 A-C). Image analyses confirmed that the cell density per area increased over time (Figure 3 G). Moreover, to verify the formation of tight junctions, indirect immunofluorescence against Claudin 5 protein was performed at day 7 of culture. Confocal microscopy images showed that bEnd.3 cells were able to express Claudin 5 protein, prevalently localized around the cell boundaries, thus indicating the formation of tight junctions (Figure 3 H). In line with these considerations, we observed a plateau starting after 4 days and completing at around day 7 by measuring the TEER of the system over culture time (Figure 4). These data demonstrated the capability of the microfluidic device to allow the growth and the correct formation of the confluent brain endothelial layer.

Nanoparticle transport across the BBB

A further validation of the model was carried out in order to assess the capability of the cell layer to remain intact after the passage of nanoparticles during the experiment in flow conditions. In particular, the aim of these tests was to find at least one stable condition in terms of flow rate and NP concentration where to perform the transcytosis experiment with functionalized and non-functionalized NPs without affecting the integrity of the cell layer. Transport experiments were performed after 7 days of static cell culture conditions. The device was connected to a syringe pump and the cells were subjected to two different flow rates (5 and 25 µl/min) which fell in the typical

range of flow rates reported in literature (Booth & Kim 2014; Prabhakarpandian et al. 2013). In order to validate the stability of the BBB microfluidic device for nanoparticle transport studies, we performed NP transcytosis experiments both in the presence and in the absence of the confluent cell layer under flow for 3 hours. Experiments were carried out by diluting NPs at a concentration of 9.20×10^{10} NP/ml in buffered cell culture medium. As shown in Figure 5, in the absence of the cell layer (blank filter), the percentage of transported NPs through the membrane at 5 µl/min was about 7 times higher than the transported NPs at 25 µl/min. Specifically, it was 13.45% at 5 µl/min and 1.96% at 25 µl/min. In presence of the confluent cell layer, the trend was inverted and the percentage of transported NPs decreased. In particular, the percentage of transported NPs at 5 µl/min was 2.72%, significantly lower than 7.33% found at 25 µl/min. We hypothesized that these results could depend on a rupture of the endothelial layer as a result of the combination of high flow rate and high NP concentration. Therefore, in order to understand the effect of the NP concentration on the integrity of the cell layer, we performed the transcytosis experiment at the higher flow rate (25 µl/min), by using an NP suspension at a concentration of 1.84×10^{10} NP/ml that was 5 times lower than the previous experiments and corresponded to the same number of NPs per unit of time as the experiment at 5 µl/min. Results shown in Figure 6 A indicated that after 3 hours under 25 µl/min flow conditions, the percentage of transported NPs was 9.9% with the cell-free filter, decreasing to 3.44% in the presence of the cell layer. In these conditions, we obtained results quite similar to those obtained at a five-time lower flow rate (5 µl/min) with a five-time higher NP concentration (9.20×10^{10} NP/ml). In fact, we obtained 3.44% of transported NPs at 25 µl/min by using NP concentration of 1.84×10^{10} NP/ml and 2.72% at 5 µl/min by using 9.20×10^{10} NP/ml, in the presence of the cell layer (Figure 6 B). We performed one-way ANOVA statistical analysis to verify the significance of these two values and we did not find a statistical difference ($p = 0.17$).

Taken altogether, these findings indicate that: i) the presence of the layer hinders the passage of nanoparticles across the filter; ii) the integrity of the cell layer depends on a right combination

https://doi.org/10.1002/bit.26221

between the concentration of the nanoparticles and the flow rate. Since our aim was not to validate the device in different conditions of speed, but to assess that even in flow conditions there is a different behavior between functionalized and not functionalized NPs, we focused on 5 µl/min flow rate where we could use a higher concentration of NPs which resulted safe for the cell layer integrity as also confirmed by TEER analysis. In particular, TEER results indicated no significant change along the 3 hours of experiment (Figure S4). Moreover, this flow rate value corresponding to 0.15 dynes/cm^2, fell in the physiological range (0.01 to 10 dynes/cm^2) (Luissint et al. 2013). At this flow rate, we also tested transport of standard molecules, such as bovine serum albumin (BSA) and obtained a strong reduction of the movement from the device with no cell layer to the device in the presence of the cell layer, as in the case of the NP transport analysis (Figure S5).

Effect of gH625 peptide on nanoparticle transport across the BBB

Several works reported that NPs enter the cells using a cell-mediated mechanism, called endocytosis. After endocytosis, endosomes can deliver their cargo across the cell by transcytosis processes. Alternatively, these vesicles can also be sent to the lysosomes for degradation. It has been already demonstrated that the gH625 is able to transport different cargos such as liposomes and quantum dots across cells (Falanga et al. 2011). In a previous work, the surface of fluorescent aminated polystyrene NPs was functionalized with the gH625 and the transport across static *in vitro* BBB models was investigated. Results demonstrated that gH625 NPs translocated efficiently across cell membranes and cell internalization did not seem to exclusively involve classical endocytosis mechanisms. In fact, the conjugation with the gH625 facilitated the delivery of nanoparticles across the BBB, leading to significantly higher cell uptake and crossing, decreasing lysosomal accumulation (Guarnieri et al. 2013). Based on these previous observations, we tested the capability of the gH625 to enhance NP transport across the BBB layer in flow conditions, at 5 µl/min flow rate, which was in the range of the flow rates in the blood capillaries and was high enough to guarantee a measurable amount of NPs along the experiment. NP concentration was fixed as in the

previous experiment at 9.20×10^{10} NP/ml. Figure 7 A shows the comparison of transported blank and gH625-NPs. As reported, the gH625 increased about two times the transport of NPs through the BBB (6.13% compared to 2.72% of non-functionalized blank NPs). Looking at the cell layer, we observed the adhesion of blank and gH625-nanoparticles after the flow experiments (Figure 7 B-E). Data show an about two-fold increment of adhered gH625-NPs compared to blank NPs (Figure 7 F) thus indicating a higher affinity of functionalized nanoparticles to the cell membrane than blank ones in dynamic conditions. Actually, the gH625 peptide shows a particular tropism for cell membrane cholesterol (Guarnieri et al. 2015). It is likely that this property may promote the interaction of the gH625-functionalized nanoparticles with the cells and, as a consequence, their adhesion to the cell membrane also in flow conditions. The linearity of the graph expressing the percentage of transported NPs over time may be an indication of the integrity of the cell layer upon the 3 hours of experiment. As a confirmation of the stability of the layer, TEER was also measured. Results indicated no significant change in TEER values along the 3 hours of experiment (Figure S4).

Conclusions

In conclusion, we designed and produced a microfluidic system in order to study the effect of flow conditions in controlling the interaction of gH625-functionalized nanoparticles with a BBB model *in vitro*. We first optimized the protocol of cell seeding to allow the cell growth and the formation of a confluent brain endothelial layer. Data clearly demonstrated that cells were able to grow and to reach the confluence in the microfluidic system by forming tight junctions. Then, the device was validated at 5 µl/min working flow rate showing the capability of the model to remain intact after the passage of nanoparticles in these experimental conditions by TEER analysis. As expected, the presence of the cell layer hindered the transport of nanoparticles across the porous membrane. Finally, crossing experiments demonstrated that the functionalization of nanoparticles with the

https://doi.org/10.1002/bit.26221

gH625 peptide contributed to enhance the BBB crossing even in flow conditions. The system allowed reproducibility of experiments and permitted the quantification of transport of molecules and nanoparticles across the BBB *in vitro*.

Acknowledgements

The authors warmly wish to thank Valentina La Tilla and Stefano Critelli for their contribution in the preparation of the Table of Contents and Roberta Infranca for her helpful proofreading.

https://doi.org/10.1002/bit.26221

References

Avdeef, A., 2011. How well can in vitro brain microcapillary endothelial cell models predict rodent in vivo blood–brain barrier permeability? *European Journal of Pharmaceutical Sciences*, 43(3), pp.109–124.

Booth, R. & Kim, H., 2012. Characterization of a microfluidic in vitro model of the blood-brain barrier (μBBB). *Lab on a Chip*, 12(10), p.1784.

Booth, R. & Kim, H., 2014. Permeability Analysis of Neuroactive Drugs Through a Dynamic Microfluidic In Vitro Blood–Brain Barrier Model. *Annals of Biomedical Engineering*, 42(12), pp.2379–2391.

Cardoso, F.L., Brites, D. & Brito, M.A., 2010. Looking at the blood–brain barrier: Molecular anatomy and possible investigation approaches. *Brain Research Reviews*, 64(2), pp.328–363.

Chen, P.C. et al., 2014. Optimization of micromilling microchannels on a polycarbonate substrate. *International Journal of Precision Engineering and Manufacturing*, 15(1), pp.149–154.

Cucullo, L. et al., 2005. Drug delivery and in vitro models of the blood-brain barrier. *Current opinion in drug discovery & development*, 8(1), pp.89–99.

Falanga, A. et al., 2011. A peptide derived from herpes simplex virus type 1 glycoprotein H: membrane translocation and applications to the delivery of quantum dots. *Nanomedicine : nanotechnology, biology, and medicine*, 7(6), pp.925–34.

Galdiero, S., Falanga, A., Vitiello, M., Raiola, L., et al., 2008. Analysis of a membrane interacting region of herpes simplex virus type 1 glycoprotein H. *The Journal of biological chemistry*, 283(44), pp.29993–30009.

Galdiero, S. et al., 2007. Evidence for a role of the membrane-proximal region of herpes simplex

https://doi.org/10.1002/bit.26221

virus type 1 glycoprotein H in membrane fusion and virus inhibition. *ChemBioChem*, 8(8), pp.885–895.

Galdiero, S. et al., 2005. Fusogenic domains in herpes simplex virus type 1 glycoprotein H. *The Journal of biological chemistry*, 280(31), pp.28632–43.

Galdiero, S. et al., 2012. Intracellular delivery: exploiting viral membranotropic peptides. *Current drug metabolism*, 13(1), pp.93–104.

Galdiero, S., Falanga, A., Vitiello, M., D'Isanto, M., et al., 2008. Peptides containing membrane-interacting motifs inhibit herpes simplex virus type 1 infectivity. *Peptides*, 29, pp.1461–1471.

Galdiero, S. et al., 2008. The identification and characterization of fusogenic domains in herpes virus glycoprotein B molecules. *ChemBioChem*, 9(5), pp.758–767.

Galdiero, S. et al., 2010. The presence of a single N-terminal histidine residue enhances the fusogenic properties of a membranotropic peptide derived from herpes simplex virus type 1 glycoprotein H. *Journal of Biological Chemistry*, 285(22), pp.17123–17136.

Guarnieri, D. et al., 2013. Shuttle-Mediated Nanoparticle Delivery to the Blood-Brain Barrier. *Small*, 9(6), pp.853–862.

Guarnieri, D. et al., 2015. Surface decoration with gH625-membranotropic peptides as a method to escape the endo-lysosomal compartment and reduce nanoparticle toxicity. *Nanotechnology*, 26(41), p.415101.

Hatherell, K. et al., 2011. Development of a three-dimensional, all-human in vitro model of the blood-brain barrier using mono-, co-, and tri-cultivation Transwell models. *Journal of Neuroscience Methods*, 199(2), pp.223–229.

Huh, D., Hamilton, G.A. & Ingber, D.E., 2011. From 3D cell culture to organs-on-chips. *Trends in*

https://doi.org/10.1002/bit.26221

Cell Biology, 21(12), pp.745–754.

Luissint, A. et al., 2013. Tight junctions at the blood brain barrier : physiological architecture and disease-associated dysregulation.

van der Meer, A.D. et al., 2010. Analyzing shear stress-induced alignment of actin filaments in endothelial cells with a microfluidic assay. *Biomicrofluidics*, 4(1), p.011103.

Paolinelli, R. et al., 2011. The molecular basis of the blood brain barrier differentiation and maintenance. Is it still a mystery? *Pharmacological Research*, 63(3), pp.165–171.

Patabendige, A., Skinner, R. a. & Abbott, N.J., 2013. Establishment of a simplified in vitro porcine blood-brain barrier model with high transendothelial electrical resistance. *Brain Research*, 1521, pp.1–15.

Prabhakarpandian, B. et al., 2013. SyM-BBB: a microfluidic Blood Brain Barrier model. *Lab Chip*, 13(6), pp.1093–1101.

Rusciano, G. et al., 2011. Label-Free Probing of G-Quadruplex Formation by Surface-Enhanced Raman Scattering. , pp.6849–6855.

Tarallo, R. et al., 2011. Clickable functionalization of liposomes with the gH625 peptide from Herpes simplex virus type I for intracellular drug delivery. *Chemistry (Weinheim an der Bergstrasse, Germany)*, 17(45), pp.12659–68.

Vecchione, R. et al., 2016. From square to circular polymeric microchannels by spin coating technology: a low cost platform for endothelial cell culture. *Biofabrication*, 8(2), p.025005.

Vitiello, G. et al., 2011. Lipid composition modulates the interaction of peptides deriving from herpes simplex virus type I glycoproteins B and H with biomembranes. *Biochimica Et Biophysica Acta-Biomembranes*, 1808(10), pp.2517–2526.

https://doi.org/10.1002/bit.26221

Wang, J.D. et al., 2016. Organization of Endothelial Cells, Pericytes, and Astrocytes into a 3D Microfluidic in vitro Model of the Blood-Brain Barrier. *Molecular Pharmaceutics*, p.acs.molpharmaceut.5b00805.

Yeon, J.H. et al., 2012. Reliable permeability assay system in a microfluidic device mimicking cerebral vasculatures. *Biomedical Microdevices*, 14(6), pp.1141–1148.

https://doi.org/10.1002/bit.26221

List of Figures

Figure 1. Schematic representation of the BBB microfluidic system (A), indicating (1) the bottom channel, (2) the polyester membrane, (3) the top channel, (4) the Nanoport UPCHURCH® connectors, (5) the collecting chamber and (6) the inlets for electrodes. Picture of the fabricated chip (B) and SEM image of the device cross-section showing top and bottom channel alignment and the sandwiched membrane (C).

Figure 2. Phase contrast microscopy pictures of the endothelial cell layer in the microfluidic system channel 1 (A), 3 (B) and 7 (C) days after cell seeding. Bar 100 μm.

Figure 3. Confocal microscopy images of confluent bEnd.3 cell layer after 7 days from cell seeding. Actin cytoskeleton stained with Phalloidin (red) (A, D); nuclei stained by DAPI (blue) (B, E); bright-field images of the polyester filter (C, F). Image acquisition was performed with a 10× dry objective. Zoomed images shown in panels A-C (D-F). Quantification of cell density over culture time evaluated by ImageJ analysis software (G). Tight junctions (green) and nuclei (blue) staining by anti- Claudin 5 primary antibodies and DAPI, respectively. Images were acquired with a 25× water-immersion objective (H). Bar 50 μm.

Figure 4. Electrical circuit model showing the resistance of the medium (R_{medium}), the resistance of the cells (R_{TEER}), the capacitance of the cell membranes (C_{Cl}) and the dual layer capacitance of Pt electrodes (C_{El}) (A). TEER values over culture time to establish endothelial cell layer formation (B).

Figure 5. Effect of flow rate on NP transport across the endothelial cell layer. Percentages of transported blank NPs *vs.* time under flow conditions in the absence (A, blank inserts) and in the presence (B, cell layer) of the confluent cell layer. Experiments were performed at two different flow rates (5 and 25 μl/min) with 9.20×10^{10} NP/ml concentration. Percentages of transported blank NPs after 3 hours under 5 μl/min flow rate, in the absence and in the presence of the confluent cell

Biotechnology & Bioengineering
https://doi.org/10.1002/bit.26221

layer (C). Confocal microscopy images of blank NPs in bEnd.3 cells after 3 hours under 5 µl/min flow rate. Green represents blank NPs and blue represents nuclei. Bar 10 µm.

Figure 6. Effect of nanoparticle concentration on transport across the endothelial cell layer. Percentages of transported blank NPs after 3 hours at 25 µl/min flow rate with 1.84×10^{10} NP/ml concentration in the absence and in the presence of the confluent cell layer (A). Comparison of transported blank NPs across the cell layer after 3 hours at 5 and 25 µl/min flow rates with NP concentrations of 9.20×10^{10} and 1.84×10^{10} NP/ml, respectively (B).

Figure 7. Effect of nanoparticle functionalization on transport across the endothelial cell layer. Percentages of transported blank and gH625-NPs over time under 5 µl/min flow rate with 9.20×10^{10} NP/ml concentration (A). Confocal images of the confluent cell layer in the microfluidic system at the end of the experiment with blank NPs (B) and gH625-NPs (C). D and E are merged images of actin cytoskeleton (red), nuclei (blue) and NPs (green) channels. Percentages of blank and gH625-NP fluorescence signal per image area evaluated by ImageJ analysis software (F). Data are reported as mean ± standard deviation (SD) (n = 10), *** $P < 0.0001$. Bar 50 µm.

https://doi.org/10.1002/bit.26221

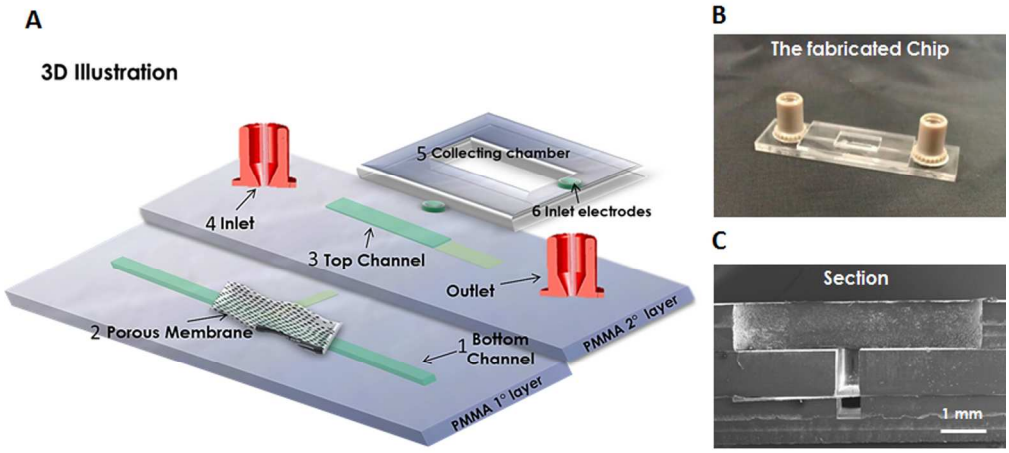

Figure 1. Schematic representation of the BBB microfluidic system (A), indicating (1) the bottom channel, (2) the polyester membrane, (3) the top channel, (4) the Nanoport UPCHURCH® connectors, (5) the collecting chamber and (6) the inlets for electrodes. Picture of the fabricated chip (B) and SEM image of the device cross section showing top and bottom channel alignment and the sandwiched membrane (C).

226x105mm (300 x 300 DPI)

Biotechnology & Bioengineering
https://doi.org/10.1002/bit.26221

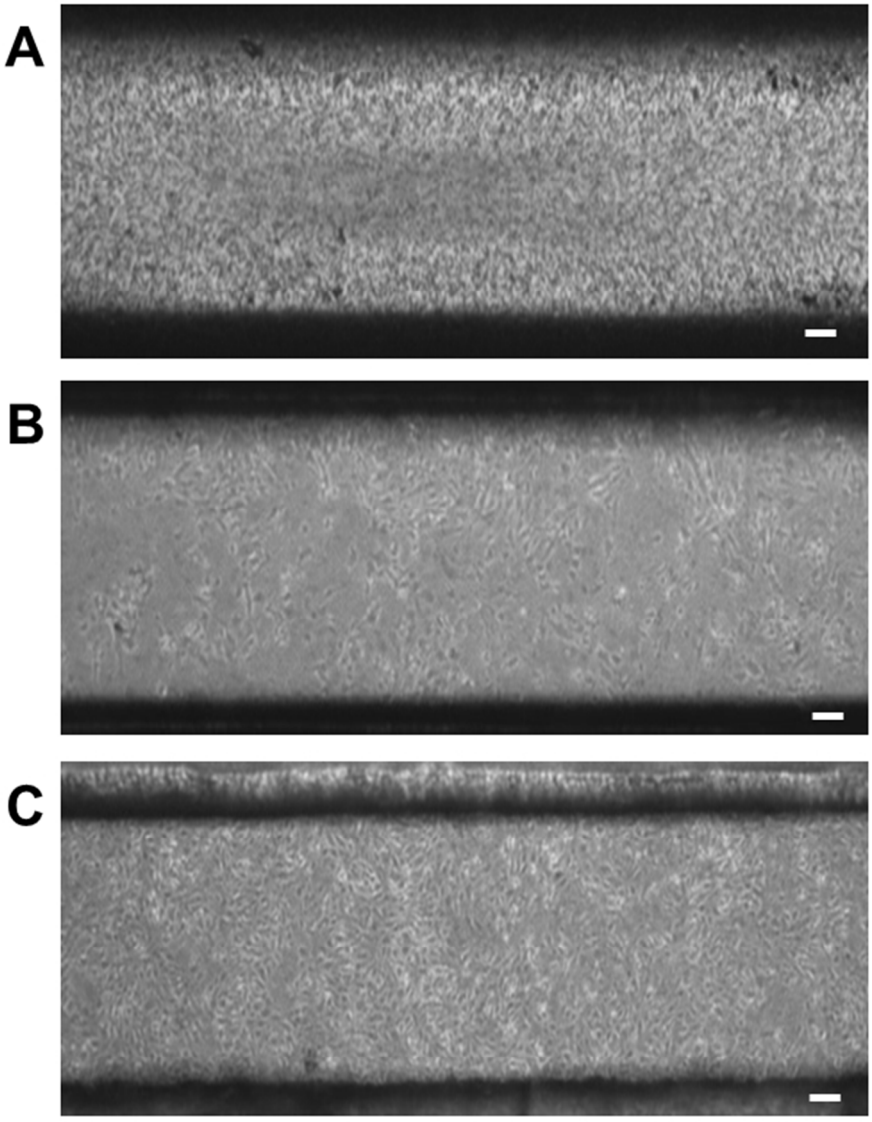

Figure 2. Phase contrast microscopy pictures of endothelial cell layer in the microfluidic system channel after 1 (A), 3 (B) and 7 (C) days from cell seeding. Bar 100 μm.

57x70mm (300 x 300 DPI)

https://doi.org/10.1002/bit.26221

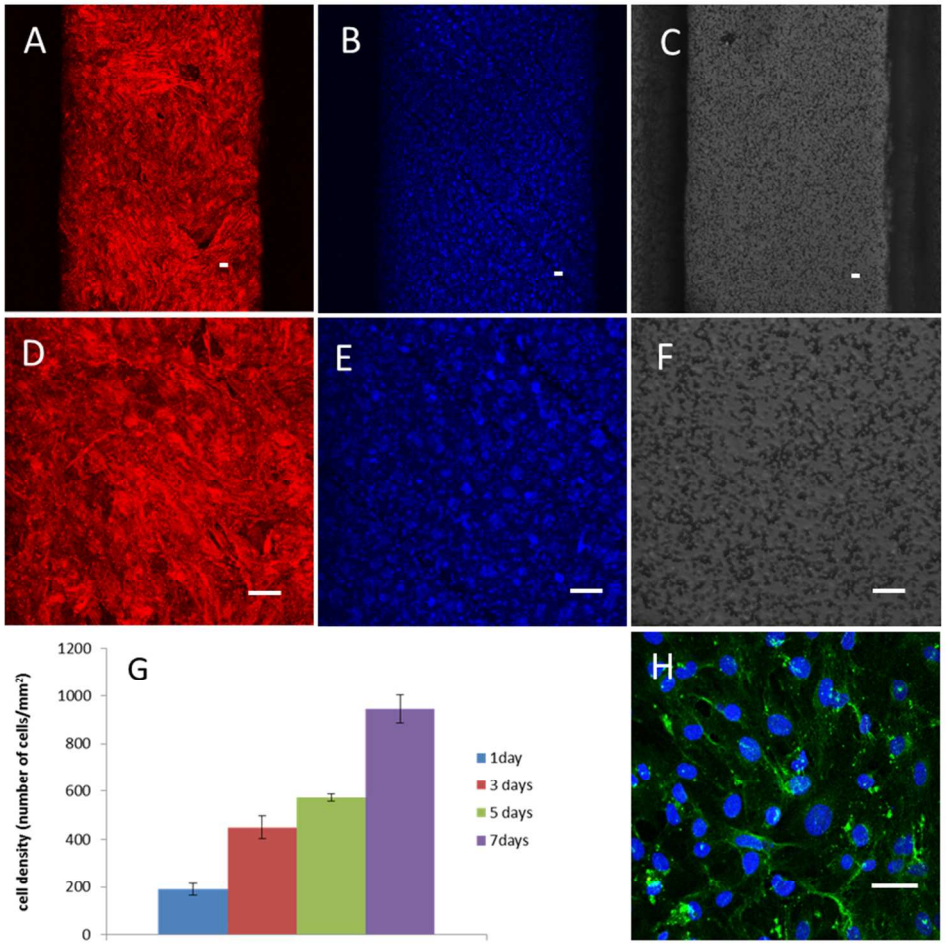

Figure 3. Confocal microscopy images of 7-day growth confluent bEnd.3 cell layer. Actin cytoskeleton stained with Phalloidin (red) (A, D); nuclei stained by DAPI (blue) (B, E); bright-field images of the polyester filter (C, F). Image acquisition was performed with a 10× dry objective. Zoomed images shown in panels A-C (D-F). Quantification of cell density over culture time evaluated by ImageJ analysis software (G). Tight junctions (green) and nuclei (blue) staining by anti- Claudin 5 primary antibodies and DAPI, respectively. Images were acquired with a 25× water-immersion objective (H). Bar 50 μm.

79x79mm (300 x 300 DPI)

Biotechnology & Bioengineering
https://doi.org/10.1002/bit.26221

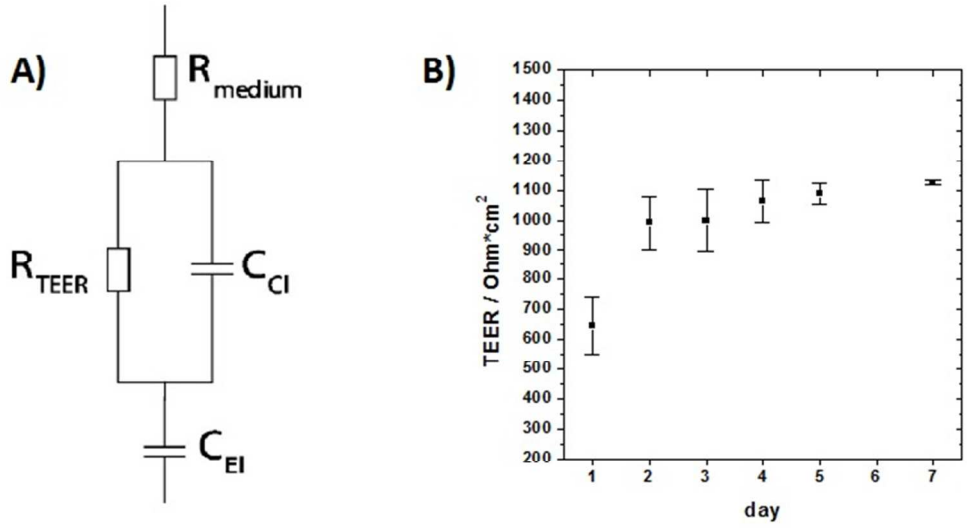

Figure 4. Electrical circuit model showing the resistance of the medium (Rmedium), the resistance of the cells (RTEER), the capacitance of the cell membranes (CCl) and the dual layer capacitance of Pt electrodes (CEl) (A). TEER values over culture time to establish endothelial cell layer formation (B).

56x33mm (300 x 300 DPI)

https://doi.org/10.1002/bit.26221

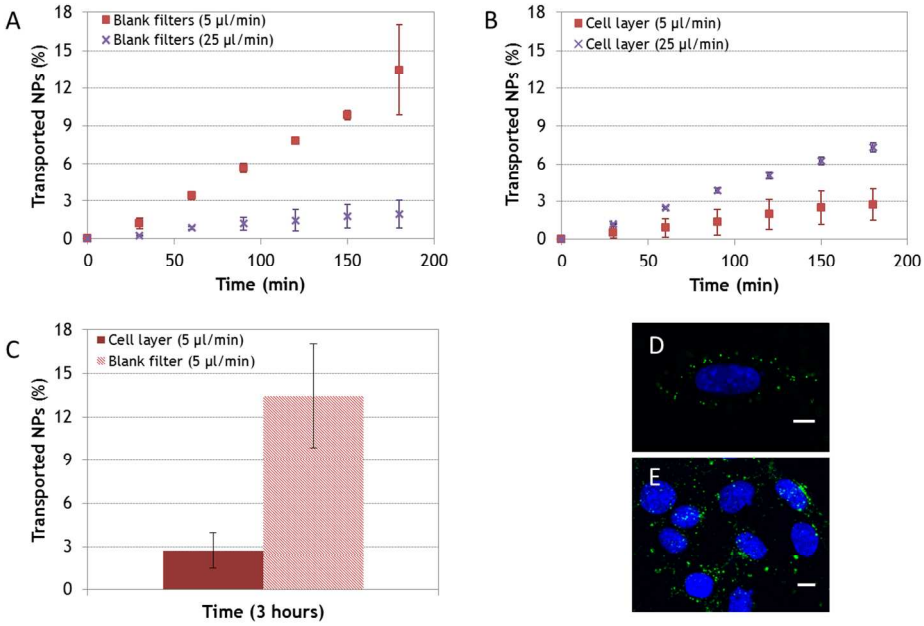

Figure 5. Effect of flow rate on NP transport across the endothelial cell layer. Percentages of transported blank NPs versus time under flow conditions in absence (A, blank inserts) and in presence (B, cell layer) of the confluent cell layer. Experiments were performed at two different flow rates (5 and 25 µl/min) with 9.20 × 1010 NP/ml concentration. Percentages of transported blank NPs after 3 hours under 5 µl/min flow rate, in absence and in presence of the confluent cell layer (C). Confocal microscopy images of blank NPs in bEnd.3 cells after 3 hours under 5 µl/min flow rate. Green represents blank NPs and blue represents nuclei. Bar 10 µm.

119x80mm (300 x 300 DPI)

Biotechnology & Bioengineering
https://doi.org/10.1002/bit.26221

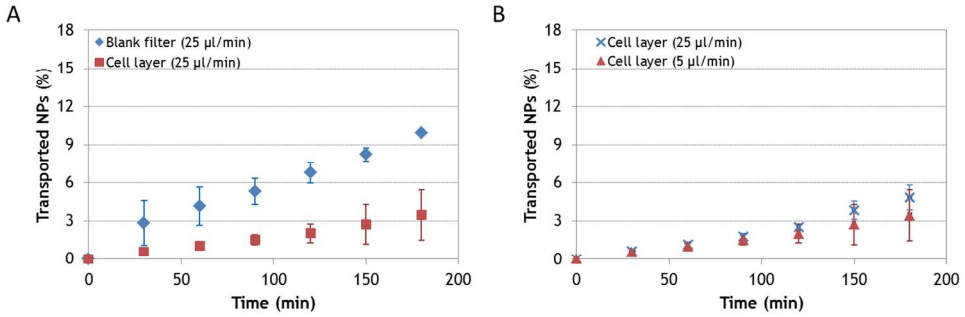

127x46mm (300 x 300 DPI)

https://doi.org/10.1002/bit.26221

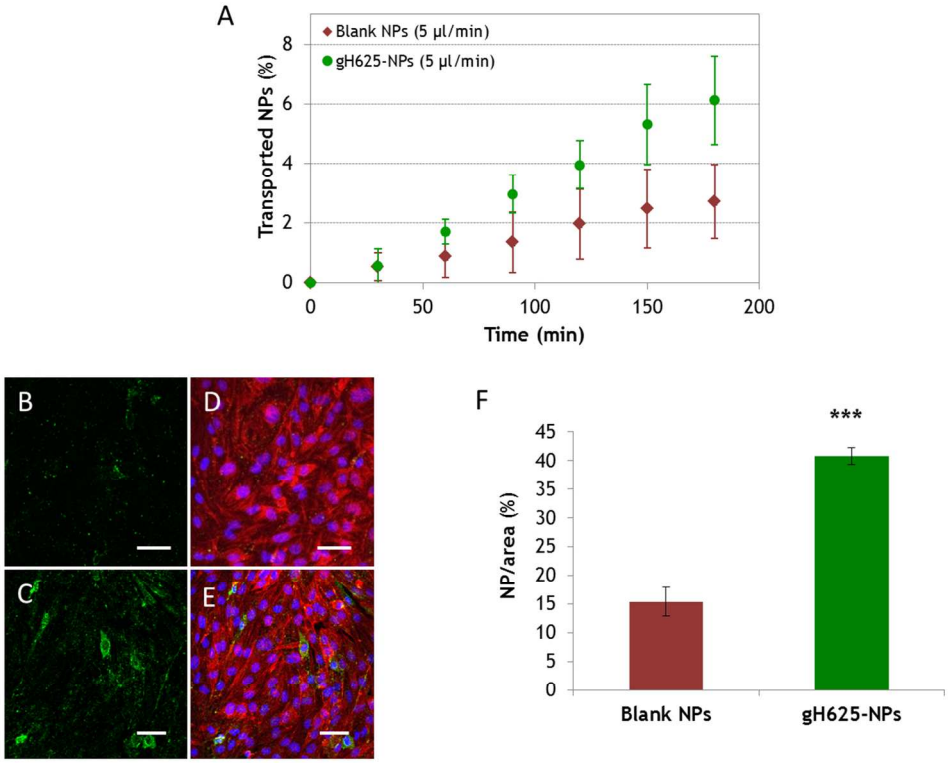

Figure 7. Effect of nanoparticle functionalization on transport across the endothelial cell layer. Percentages of transported blank and gH625-NPs over time under 5 µl/min flow rate with 9.20 × 1010 NP/ml concentration (A). Confocal images of the confluent cell layer in the microfluidic system at the end of the experiment with blank NPs (B) and gH625-NPs (C). D and E are merged images of actin cytoskeleton (red), nuclei (blue) and NPs (green) channels. Percentages of blank and gH625-NP fluorescence signal per image area evaluated by ImageJ analysis software (F). Data are reported as mean ± standard deviation (SD) (n = 10), *** P < 0.0001. Bar 50 µm.

106x86mm (300 x 300 DPI)

Biotechnology & Bioengineering
https://doi.org/10.1002/bit.26221

SUPPORTING INFORMATION

Shuttle-mediated nanoparticle transport across an *in vitro* brain endothelium under flow conditions

RUNNING TITLE: Functionalized-NP transport through a BBB on a chip

Andrea P. Falanga[1], Gabriele Pitingolo[1], Maurizio Celentano[1], Armando Cosentino[1], Pietro Melone[1], Raffaele Vecchione[1,*], Daniela Guarnieri[1,*], Paolo A. Netti[1,2,3]

[1]*Center for Advanced Biomaterial for Health Care (CABHC), Istituto Italiano di Tecnologia, Largo Barsanti e Matteucci 53, Napoli, Italy*

[2]*Centro di Ricerca Interdipartimentale sui Biomateriali (CRIB), Università di Napoli Federico II, Piazzale Tecchio 80, Napoli, Italy*

[3]*Dipartimento di Ingegneria, Università di Napoli Federico II, Piazzale Tecchio 80, Napoli, Italy*

* Corresponding authors: daniela.guarnieri@iit.it ; raffaele.vecchione@iit.it

https://doi.org/10.1002/bit.26221

Simulations

Simulations based on the Finite Element Method (FEM) were performed to verify the spontaneous direction of vertical flow through a permeable layer in place of the brain endothelial layer. To this aim, a simplified model based on the Navier Stokes equations in porous media was introduced.

The FEM-based simulation model was developed via the commercial software COMSOL Multiphysics 5.0 [COMSOL, Inc., 2013. COMSOL Multiphysics® User's Guide, Version 5.0.]. We have utilized two multiphysics modules. First of all, the laminar two-phase flow, level set interface module was introduced in the upper reservoir and consisted in the time-dependent Navier-Stokes equations and the following:

$$\frac{\partial \varphi}{\partial t} + u \cdot \nabla \varphi = \gamma \nabla \cdot \left(\varepsilon_{ls} \nabla \varphi - \varphi(1-\varphi) \frac{\nabla \varphi}{|\nabla \varphi|} \right)$$

where u is the velocity, φ is the level set variable, γ is a reinitialization parameter and ε_{ls} is a parameter controlling the liquid/air interface thickness. Simultaneously, the Navier-Stokes equations were solved for pure liquid flow in the lower channel and the reacting flow in porous media module was considered in the porous membrane.

$$\frac{\rho}{\varepsilon_p} \left(\frac{\partial u}{\partial t} + (u \cdot \nabla) \frac{u}{\varepsilon_p} \right) = \nabla \cdot \left[-pI + \frac{\mu}{\varepsilon_p} (\nabla \mathrm{u} + (\nabla u)^T) - \frac{2\mu}{3\varepsilon_p} (\nabla \cdot u) I \right] - \left(\mu \kappa^{-1} + \beta_F |u| + \frac{Q_{br}}{\varepsilon_p^2} \right) u + F$$

where ρ is the density, μ is the viscosity, p is the pressure, I is the identity matrix, F is the gravity force.

In our system, from one hand the gravity force, acting in the upper reservoir, tends to move the liquid downward from the other hand the pressure in the bottom channel tends to move the liquid in the opposite direction. The simulated membrane was characterized by two parameters: the absolute permeability and the porosity. The former is related to the transport characteristics of the homogeneous substrate and the latter is related to the presence of pores. Being the only scope of the simulation to understand the direction of the fluid flow we fixed arbitrary values of the porosity and absolute permeability as low as possible, 10^{-5} and $10^{-17} m^2$, respectively. For lower porosity the simulation did not converge while for lower permeability the results did not change. It resulted that the liquid/air interface in the reservoir moves slightly downward as the

https://doi.org/10.1002/bit.26221

maximum decrement of liquid volume is about 3% after 10 minutes (Figure S3). This is in agreement with the experiments where no variation in liquid volume is observed. In this scenario, we can exclude any particle transmigration from the bottom microchannel to the up chamber due to fluid extravasation since the spontaneous flow direction is in the opposite direction.

The presented original FEM model is helpful also for geometries characterized by a higher complexity and can be applied in the case of extravasation by implementing the parameters of the semipermeable membrane.

https://doi.org/10.1002/bit.26221

Figure S1. Pictures of the device including the electrodes (A) and a homemade Pt electrode alone.

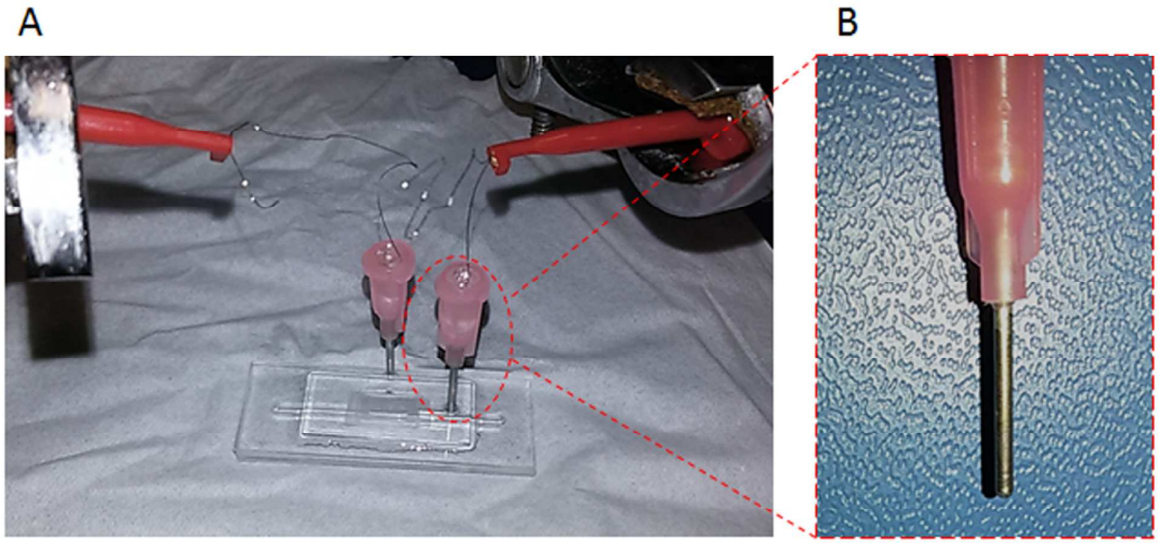

https://doi.org/10.1002/bit.26221

Figure S2. Transmission electron microscopy (TEM) images of blank NPs (A) and gH625-NPs (B). Bar 100 nm.

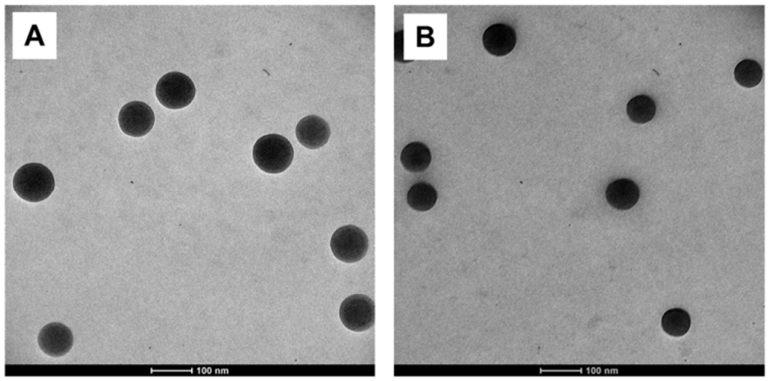

https://doi.org/10.1002/bit.26221

Figure S3. Close-up of the 2D geometry adopted for the simulations: bottom channel (channel), microchannel array, cellular membrane (membrane) and upper domain (reservoir). Simulated evolution of the liquid/air volume fraction after 10min; note the initial level (black line).

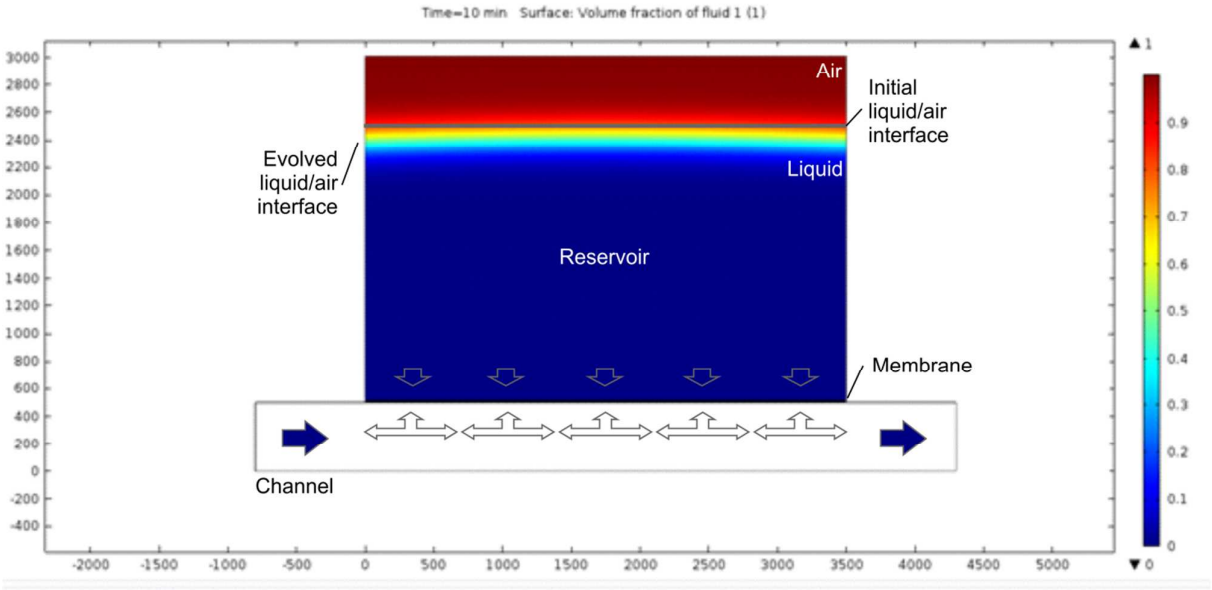

https://doi.org/10.1002/bit.26221

Figure S4. TEER analysis to validate cell layer integrity after 3 hours experiment with a 5 µl/min flow rate and 9.20×10^{10} NP/ml.

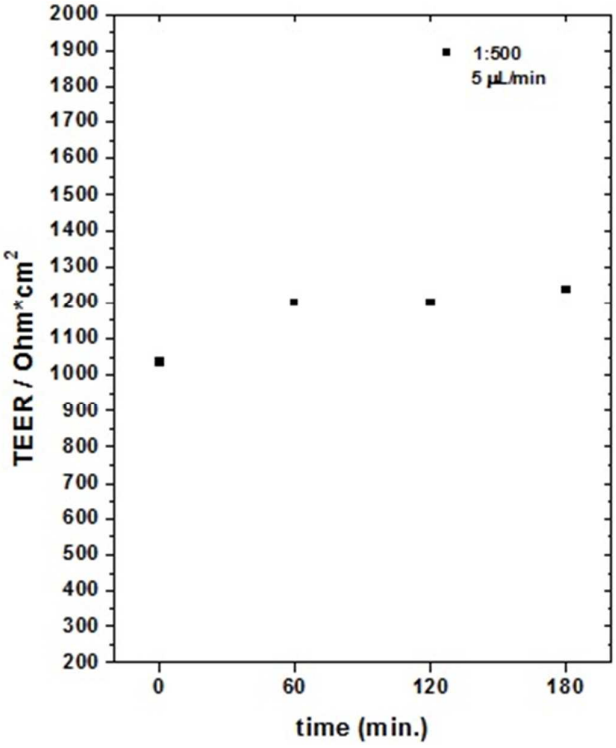

https://doi.org/10.1002/bit.26221

Figure S5. Percentages of transported FITC labeled BSA after 3 hours under 5 µl/min flow rate, in absence and in presence of the confluent cell layer.

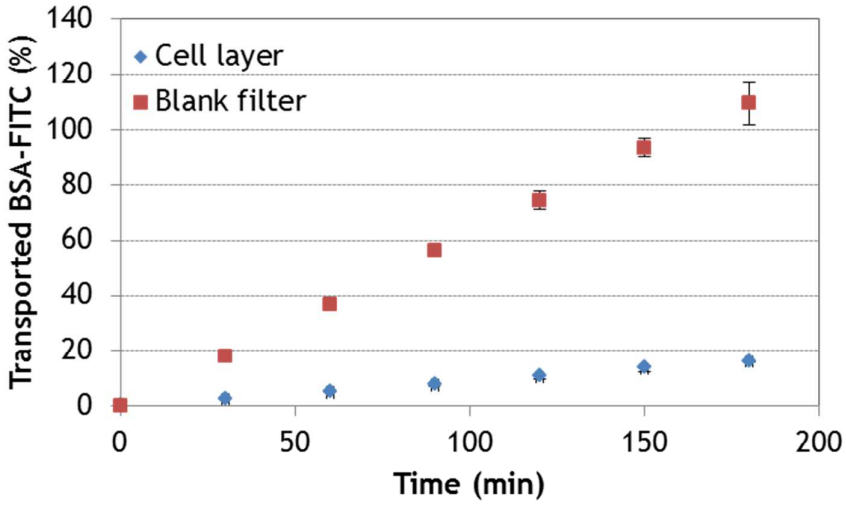

Biotechnology & Bioengineering
https://doi.org/10.1002/bit.26221

Table S1. Size, polydispersity index (PDI) and ζ-potential of blank and gH625-NPs. Data are reported as mean ± SD.

Sample	Size (nm)	PDI	Z-potential (mV)
Blank NPs	109 ± 2	0.15 ± 0.02	34 ± 1
gH625-NPs	112 ± 4	0.22 ± 0.02	24 ± 2